GSA Data Repository 2015348

Bottoms up: Sedimentary control of the deep ocean's εNd signature

April N. Abbott, Brian A. Haley, and James McManus

Additional Methods

Sample Preparation

Iron coprecipitation techniques were used to preconcentrate seawater and pore water REEs (modified from Stichel et al., 2012). Briefly, 1 mL clean ~1.0 M ferric chloride solution was added to each 20 L seawater sample and each 1 L of pore water followed by enough ultra-pure ammonia hydroxide to raise the pH of the water to 8. The water was syphoned away after iron flocculation was complete (typically 24 to 72 hours) and the remaining iron floc was rinsed with MQ water at least 3 times. Samples were then refluxed in distilled concentrated HCl and HNO_3 in a 1:1 solution for 24 to 78 hours, dried down completely and redissolved in ultrapure 6 M HCl (Stichel et al., 2012). Diethyl ether back extractions removed ~90% of the Fe from the solution. The samples were dried after ether back extractions to eliminate any remaining ether before being brought up in 1 mL 6M HCl.

Sediment, water column, and pore fluid samples were run through a series of ion exchange columns to isolate the Nd fraction for isotopic analysis. AG-1X8 resin was used first to remove Fe from the solution and therefore increase the yield and efficiency of the remaining columns. The resin was cleaned with 6 mL 6M HNO_3, 6 mL MQ, and conditioned with 6 mL 6M HCl before the sample was loaded in 1 mL 6M HCl as collection began and eluted with an additional 5 mL 6M HCl (modified from Scholz et

al., 2014). Next, cation exchange columns (1.8 mL AG50-8X HCl form resin) removed major cations. Neodymium was further isolated from other lanthanides using Ln Spec resin (modified from Pin and Zalduegui, 1997). Each column was loaded with 2 mL of 50-100 μm mesh Ln resin (Eichrom® part LN-B50-5) and cleaned with 4 mL 6M HCl and 6 mL MQ. The column was then conditioned in 4 mL 0.1M HCl before the 0.5 mL sample was loaded in 0.1M HCl, and then eluted with 15 mL 0.1M HCL and 0.25M HCl.

Flux Calculations

The benthic flux of Nd from each of our sites was calculated using the concentration gradient in the pore fluids (Abbott et al., 2015). The benthic fluxes at our sites (between 2.6 and 31 pmol cm^{-2} yr^{-1}) are in agreement with benthic flux estimates from pore fluid (between 2.8 and 36 pmol cm^{-2} yr^{-1}) and benthic chamber (2.1 pmol cm^{-2} yr^{-1}) flux calculations from the California margin (Haley and Klinkhammer, 2003). We estimated the benthic flux of Nd at our 200 m site using a linear fit with a molecular diffusion coefficient (D) value of $2.3x10^{-6}$ even though the presence of macrofauna at this site likely interferes with diffusive processes (Abbott et al., 2015). Flux calculations at our sites did not take into account the concentration of Nd in the bottom water, allowing us to maintain the independence of piston velocity in identifying the relationship between piston velocity and ΔεNd (equation 2). However, for illustrative purposes, we also calculate the flux across the sediment-water interface including the bottom water. These calculations are based on only the bottom water Nd concentration and the upper most (1.2 cm) pore fluid Nd concentration after the calculation by Haley and Klinkhammer (2003). The resulting fluxes still increase from our 200 m site (16 pmol cm^{-2} yr^{-1}) to our 1200 m site (22 pmol cm^{-2} yr^{-1}) to our 3000 m site (26 pmol cm^{-2} yr^{-1}).

Exposure Time Model

We modeled the sensitivity of the εNd_{WM} response to the benthic flux over time. Specifically, the model demonstrates how exposure time can limit εNd_{WM} alteration. The fundamental constraint is whether the observed spatial variation in water column εNd values is consistent with our measured benthic flux values. For this model, we define:

$$\varepsilon Nd_{BW}(t) = \varepsilon Nd_{BW}(t=0) \times ([Nd]_{BW,\, t=0}/[Nd]_{BW,\, t=t}) + \varepsilon Nd_{Flux}(t=0) \times ([Nd]_{Flux,\, t=0}/[Nd]_{BW,\, t=t}) \quad (4)$$

and

$$[Nd]_C = F \times t \times p \quad (5)$$

Where $[Nd]_C$ is the cumulative concentration of Nd that is derived from the benthic input, F is the flux, t is time, and p is the limit imposed on the amount of Nd as a fraction of the flux that can be added to the bottom water ($0 \leq p \leq 1$). We present the simplest of these models in the main text: a 500 year simulation for 6 scenarios, each with $\varepsilon Nd_{Flux} = -5$ and $\varepsilon Nd_{BW} = 0$, in which the amount of Nd added is equal to the cumulative flux (i.e., p=1, Figure 4). The model presented is not at steady state as there is no loss term included to conserve bottom water Nd concentrations. However, by adjusting p we can numerically conserve the Nd concentration in the water mass, and bring the model towards steady state. While conservation of concentration is possible, a realistic sink needs to be constrained both isotopically and in terms of the pattern of REEs. The constraint of the sink is tangential to the characterization of the source of Nd from the benthic flux. For this reason, we do not present the results of the steady state model. For the model presented (Figure 4) we use a constant water mass height of 2000 m for all 6 scenarios when calculating the amount of Nd in the bottom water (concentration (pmol cm^{-3}) × height (cm)). The model can be adjusted to the parameters

at each site (e.g. water column height, εNd_{Flux}, and εNd_{BW}) and can be adjusted for a balance between source and sink (i.e. steady state, p approaches 0). Currently, presenting the results of this site specific model are unwarranted given that the pore fluid εNd data presented here are the first of their kind and limited to sites on the Oregon margin. The purpose of the model at this stage is to conceptualize the influence of the benthic flux and the simplest model (presented) demonstrates how εNd might change in a water mass as it is exposed to a Nd flux from below. While the simplest model provides a crude estimate for the benthic processes that determine bottom water εNd in the North Pacific, more complex models will need to be implemented to fully describe these processes.

Additional References

Gutjahr, M., Frank, M., Stirling, C.H., Keigwin, L.D., and A.N. Halliday (2008). Tracing the Nd isotope evolution of North Atlantic Deep and Intermediate Waters in the western North Atlantic since the Last Glacial Maximum from Blake Ridge sediments. *Earth and Planetary Science Letters*, **266**, 61-77. doi: 10.1016/j.epsl.2007.10.037

Haley, B.A., and G.P. Klinkhammer (2003). Complete separation of rare earth elements from small volume seawater samples by automated ion chromatography: method development and application to benthic flux. *Marine Chemistry*, **82**, 197-220.

Haley, B.A., Frank, M., Hathorne, E., and N. Pisias (2014). Biogeochemical implications from dissolved rare earth element and Nd isotope distributions in the Gulf of Alaska. *Geochimica et Cosmochimica Acta*, **126**, 455-474. doi: 10.1016/j.gca.2013.11.0112

Piepgras, D.J., and G.J. Wasserburg (1987). Rare earth element transport in the western North Atlantic inferred from Nd isotopic observations*. *Geochimica et Cosmochimica Acta*, **51**, 1257-1271.

Pin, C. and Zalduegui, J.F.S. (1997). Sequential separation of light rare-earth elements, thorium and uranium by miniaturized extraction chromatography: Application to isotopic analyses of silicate rocks. *Analytica Chimica Acta*, **339**, 79-89.

Scholz, F., Severmann, S., McManus, J., Noffke, A., Lomnitz, U., and Hensen, C. (2014). On the isotope composition of reactive iron in marine sediments: Redox shuttle versus early diagenesis. *Chemical Geology*, **389**, 48-59. DOI 10.1016/j.chemgeo.2014.09.009

Talley, L.D., Pickard, G.L., Emery, W.J., and Swift, J.H. (2011). Descriptive Physical Oceanography: An Introduction, 6th ed., Academic Press, New York.

Vance, D., and K. Burton (1999). Neodymium isotopes in planktonic foraminifera: a record of the response of continental weathering and ocean circulation rates to climate change. *Earth and Planetary Science Letters*, **173**, 365-379.

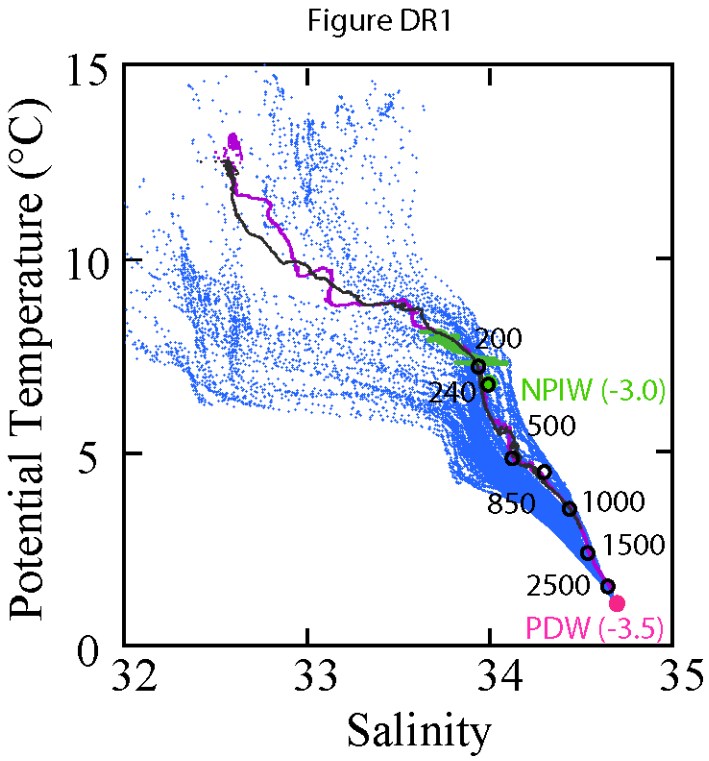

Figure DR1. Temperature plotted as a function of salinity for 200 m (green), 1200 m (black), and 3000 m (purple) sites. Blue dots are WOCE data for the eastern North Pacific (Schlitzer, R., Ocean Data View, http://odv.awi.de). Select water column depths are labeled (in meters, open circles) on the plot. Major water mass cores for North Pacific Intermediate Water (NPIW, green) and Pacific Deep Water (PDW, pink) are identified with solid circles. Water mass temperature and salinity data is from Talley et al. (2011) and the εNd of the water masses (labeled in parenthesis) is from Haley et al. (2014).

Figure DR2

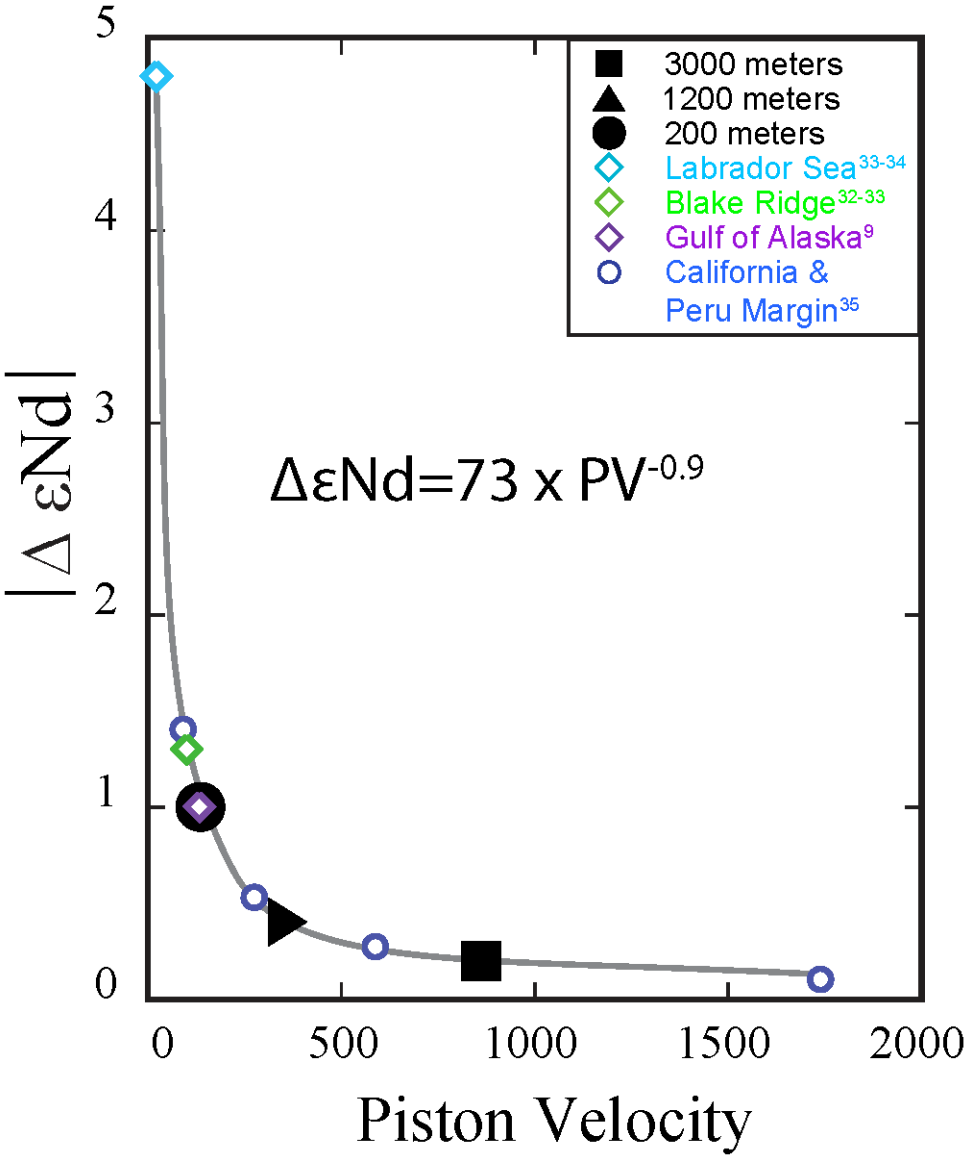

Figure DR2. |ΔεNd| plotted as a function of piston velocity (PV). The relationship between |ΔεNd| and piston velocity is described as $|\Delta\varepsilon Nd| = 73 \times PV^{-0.9}$. This relationship shows that εNd_{BW} is not altered to resemble εNd_{BW} when the piston velocity approaches zero allowing ΔεNd to retain higher values. Alternatively, |ΔεNd| will approach zero as

piston velocities increase. Filled symbols are sites where both ΔεNd and piston velocity are based on field measurements. Open diamonds are calculated piston velocities based on measured ΔεNd and $[Nd]_{BW}$. Open circles are calculated ΔεNd based on published pore water fluxes and $[Nd]_{BW}$ (Haley and Klinkhammer, 2003).

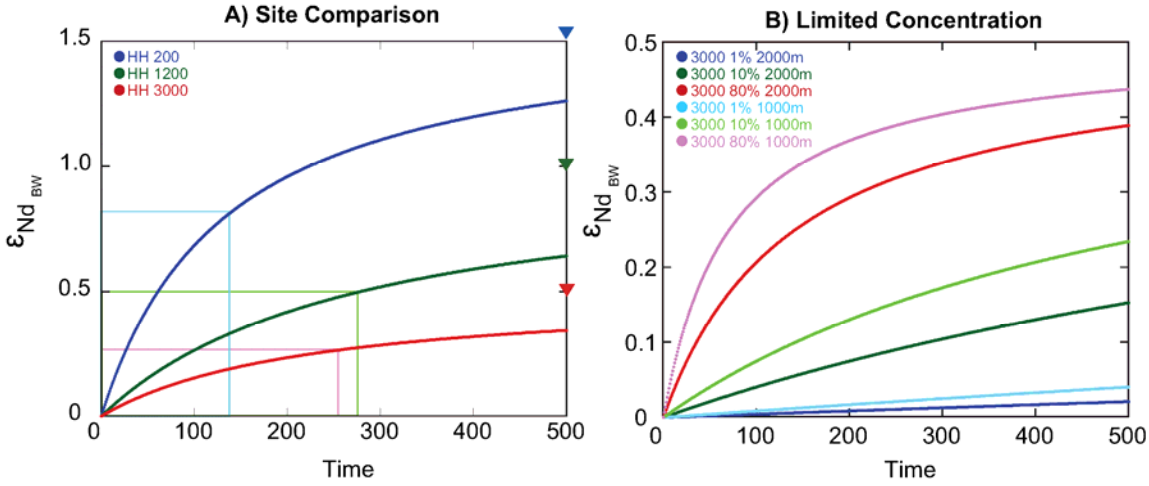

Figure DR3. A) Resulting εNd_{WM} for modeled flux scenarios representing observations at our 200 m (blue), 1200 m (green), and 3000 m sites (red). Triangles on the right axis indicate the εNd_{FLUX} for each site. The boxes indicate the time needed for the εNd_{WM} to an εNd_{WM} half way between the initial εNd_{WM} and εNd_{FLUX}. B) Resulting εNd_{WM} for modeled flux scenarios limited increases in bottom water Nd concentration of 1% (blue), 10% (green), and 80% (red) of the flux for a 2000 m water column (dark) and a 1000 m water column (light) for observed conditions at our 3000 m site.

Table DR1. Estimating Flux from Changes in Epsilon

Site	IΔεNdI	εNd_{Flux}	εNd_{BW}	F_{Nd}	$[Nd]_{BW}$	piston velocity	References
				pmol cm^{-2} yr^{-1}	pM	cm yr^{-1}	
HH3000	0.2	-1.8	-2.0	31.0	36	861	1
HH1200	0.4	-1.5	-1.9	13.0	36	361	1
HH200	1.0	-0.2	-1.2	2.6	19	137	1
Labrador Sea	4.8	-13.5	-18.3	***0.4***	20	22	2,3
Blake Ridge	1.3	-12.2	-13.5	***6.2***	62	99	4
N. Pacific GOA	1.0	-2.1	-3.1	***5.8***	43	134	5
Peru, MC84	***0.5***	n/a	n/a	7.7	29	266	6
800 m site, California	***0.3***	n/a	n/a	19.9	34	585	6
1600 m site, California	***1.4***	n/a	n/a	2.8	33	85	6
3400 m site, California	***0.1***	n/a	n/a	36.0	23	1565	6

1 This Study
2 Vance and Burton 1999
3 Piepgras and Wasserburg 1987
4 Gutjahr et al. 2008
5 Haley et al., 2014
6 Haley and Klinkhammer 2003
Bold & Italic= calculated this study

Table DR1. Results from equation 3 estimates of flux and ΔεNd from sites where either the pore water flux and the bottom water Nd concentration or the ΔεNd is published compared to sites in this study. The calculated component is in bold italics.

Table DR2. Site Descriptions

Cruise	Site	Water Depth (m)	Latitude	Longitude	Oxygen (µmol/L)	Date
OC1307a	HH200	202m	43.917	124.68	71	Jul-13
OC1210a	HH1200	1216m	43.083	124.983	20	Oct-12
	HH3000	3060m	43.867	125.633	82	Oct-12

Table DR2. Site descriptions and site locations (latitude and longitude are in decimal degrees).

Table DR3. Water Column Nd

Site	Depth	[Nd] pM	εNd
HH200	20	22	-1.6
	70	17	-1.9
	75	18	-2.3
	110	20	-1.8
	150	20	-2.3
	175	21	-1.6
	195	21	-1.7
	200	12	-1.2
HH500	420	19	-2.8
	505	17	-2.2
	515	18	-2.5
HH1200	25	22	-1.5
	300	17	-3.1
	500	15	-2.1
	600	20	-2.8
	800	31	-3.2
	900	27	-2.3
	1149	32	-2.6
	1208	36	-2.1
	1229	22	-1.9
HH3000	20	13	-1.3
	250	11	-2.6
	500	17	-2.9
	750	13	-2.4
	1000	16	-2.4
	1200	18	-2.4
	1500	20	-2.0
	2000	23	-2.3
	2500	27	-1.5
	3000	33	-2.4
	3020	36	-2.7
	3041	12	-2.0
NBPGSR10	**mean**	24.80	
n=27	**1 sigma**	3.91	
	Procedural Blank	3.5±1.8	

Table DR4. Pore water and sedimentary Nd

Site	Depth	$[Nd]_{PW}$	εNd_{PW}	$[Nd]_{BS}$	εNd_{BS}
	cm	*pM*		*µg/g sed*	
HH200	1.2	203	-0.1	13.8	-0.8
	2.5	181	-0.2	13.3	-0.8
	3.7	241	-0.2	14.1	-1.3
	4.9	264	-0.5	14.7	-1.3
	6.2	291	0.0	14.6	-2.8
	7.4	275	-0.1	14.9	-1.6
	8.6	163	-0.1	14.6	-1.4
	9.9	166	0.0	13.9	-1.8
	11.1	245	-0.2	13.1	-0.9
	13.3	313	n/a	13.0	-0.5
	15.5	398	n/a	13.0	-1.7
	17.7	277	n/a	13.7	-2.3
HH1200	1.2	289	-3.5	14.7	-1.9
	2.5	491	-2.9	16.0	-0.8
	3.7	496	-1.2	15.8	-1.7
	4.9	450	-1.3	12.9	-1.8
	6.2	357	-1.5	15.7	-2.1
	7.4	329	-1.5	15.5	-2.0
	8.6	281	-2.3	16.5	-1.0
	9.9	243	-1.6	17.0	-2.3
	11.1	205	-1.2	16.7	-2.4
HH3000	1.2	338	-1.8	17.1	-1.7
	2.5	563	-1.8	15.8	-2.0
	3.7	726	-1.6	17.4	-2.4
	4.9	724	-1.8	16.1	-2.5
	6.2	788	-2.4	21.9	-2.5
	7.4	513	-1.9	16.7	-2.5
	8.6	340	-1.8	17.3	-2.2
	9.9	212	-1.8	16.7	-2.2
	11.1	208	-1.7	16.9	-2.1